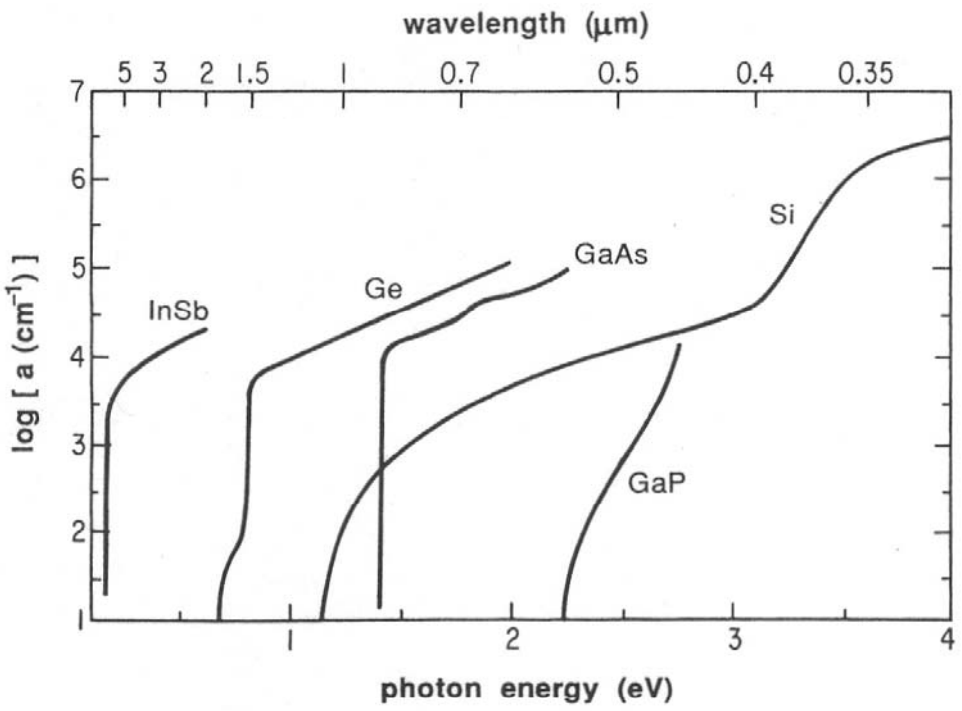

Figure 3.5. Absorption coefficients for various semiconductors, after Stillman and Wolfe (1977).

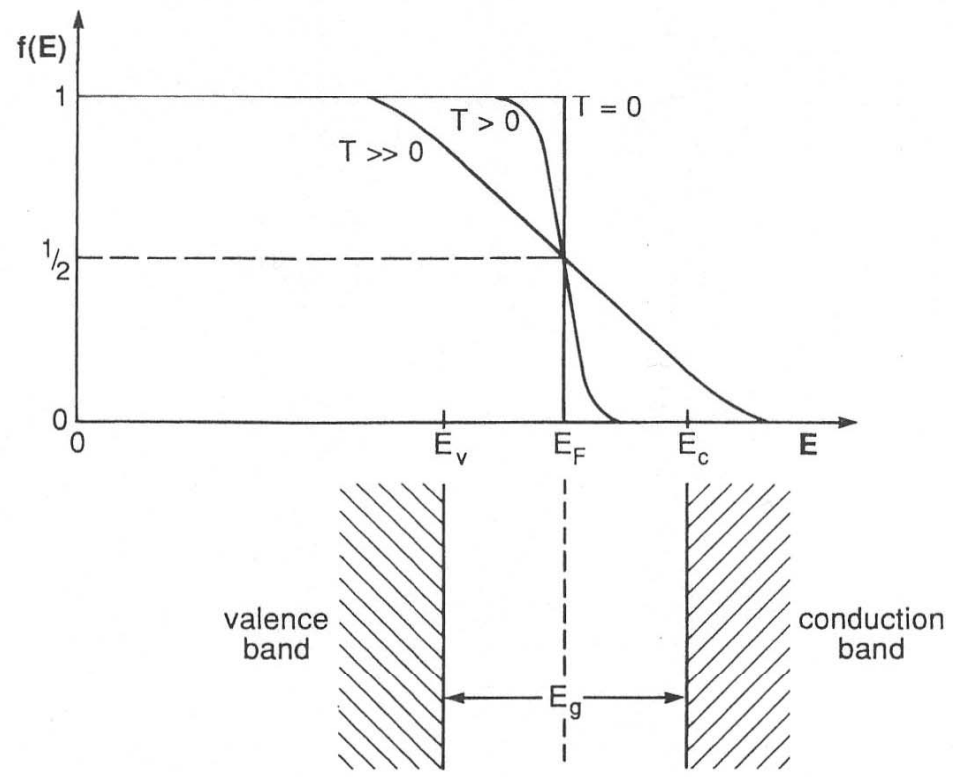

Figure 3.9. Electron probability distribution $f(E)$ as a function of temperature T, compared with an energy band diagram.

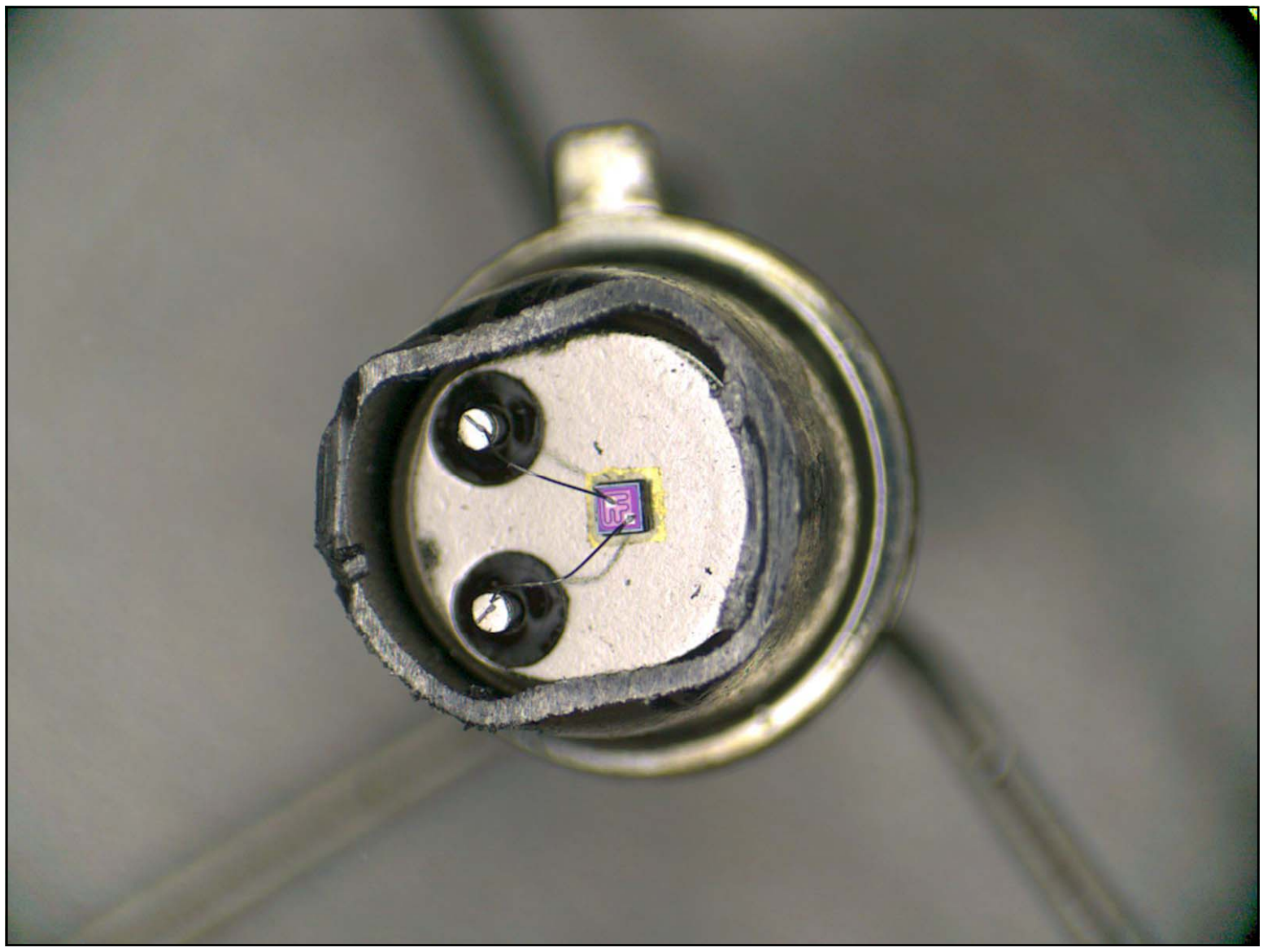

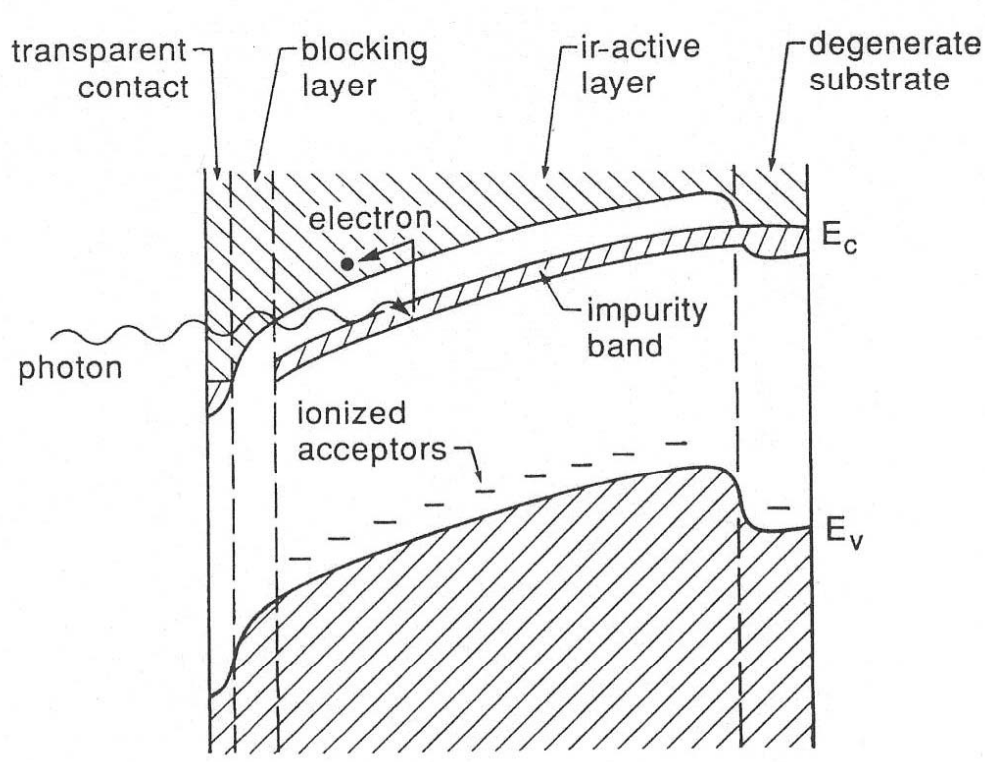

Figure 4.6. Band diagram for Si:As BIB detector.

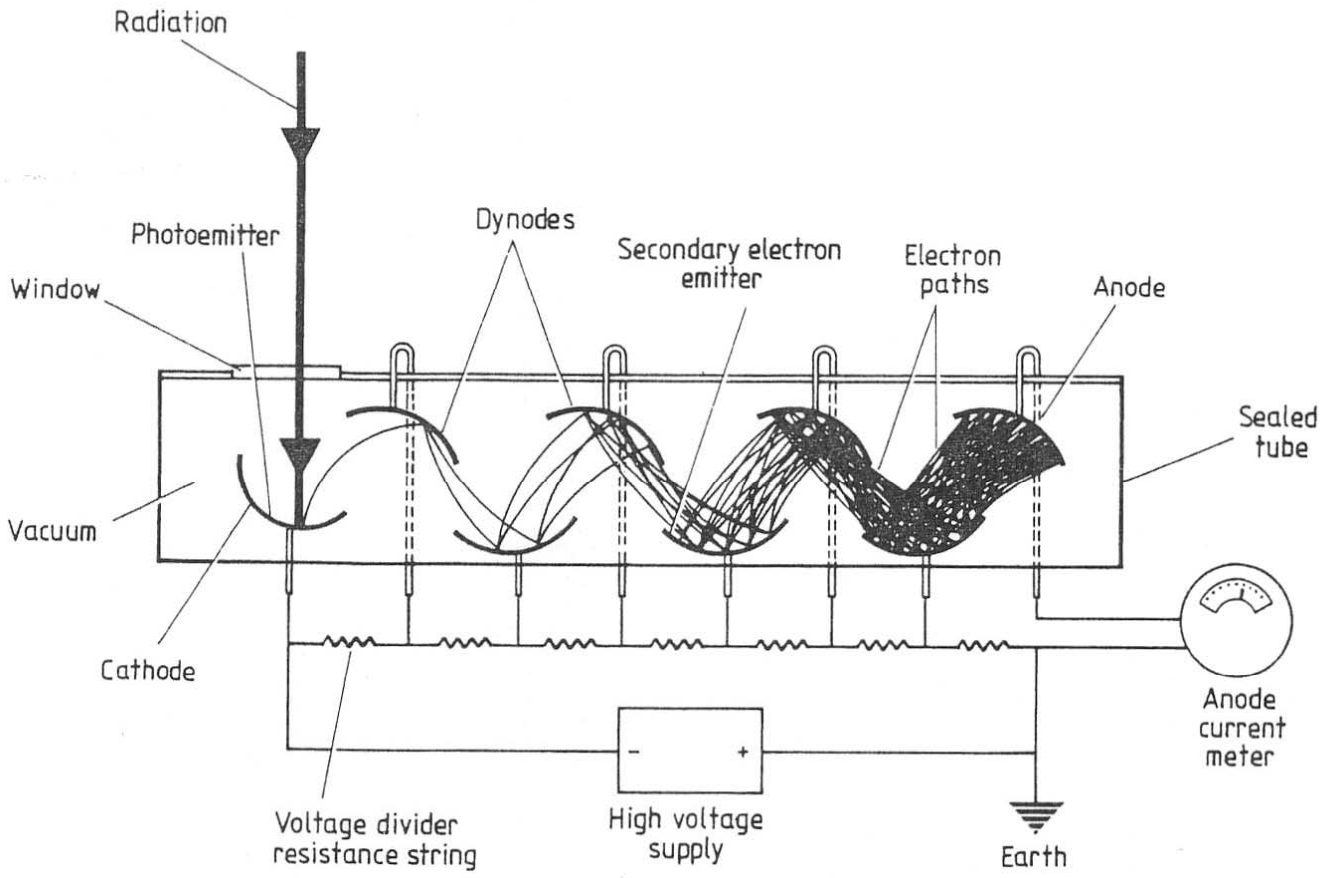

Figure 1.1.10 Schematic arrangement for a photomultiplier.

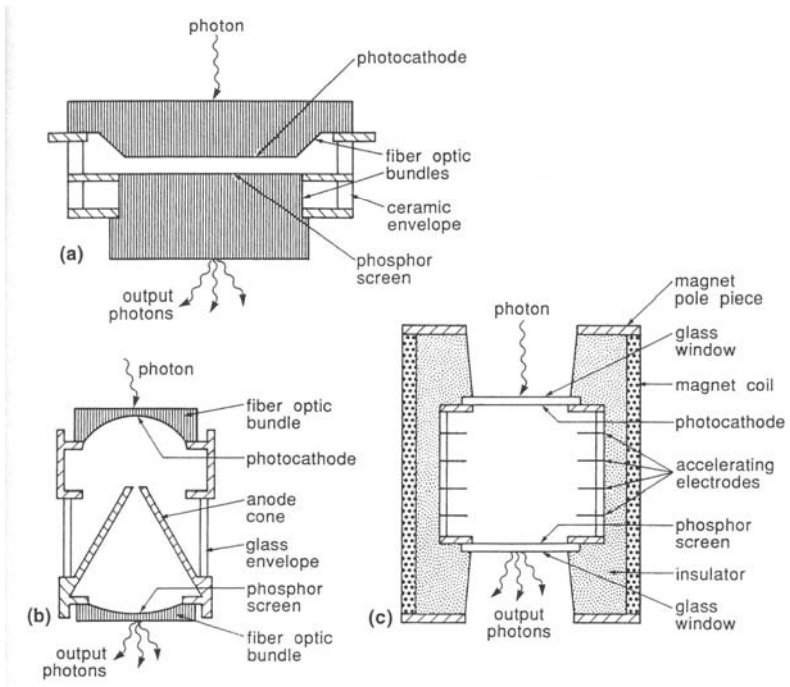

Figure 8.10. Cross-sectional diagrams of a variety of image intensifer types: (a) proximity focused; (b) electrostatically focused; and (c) magnetically focused. After Csorba (1985).

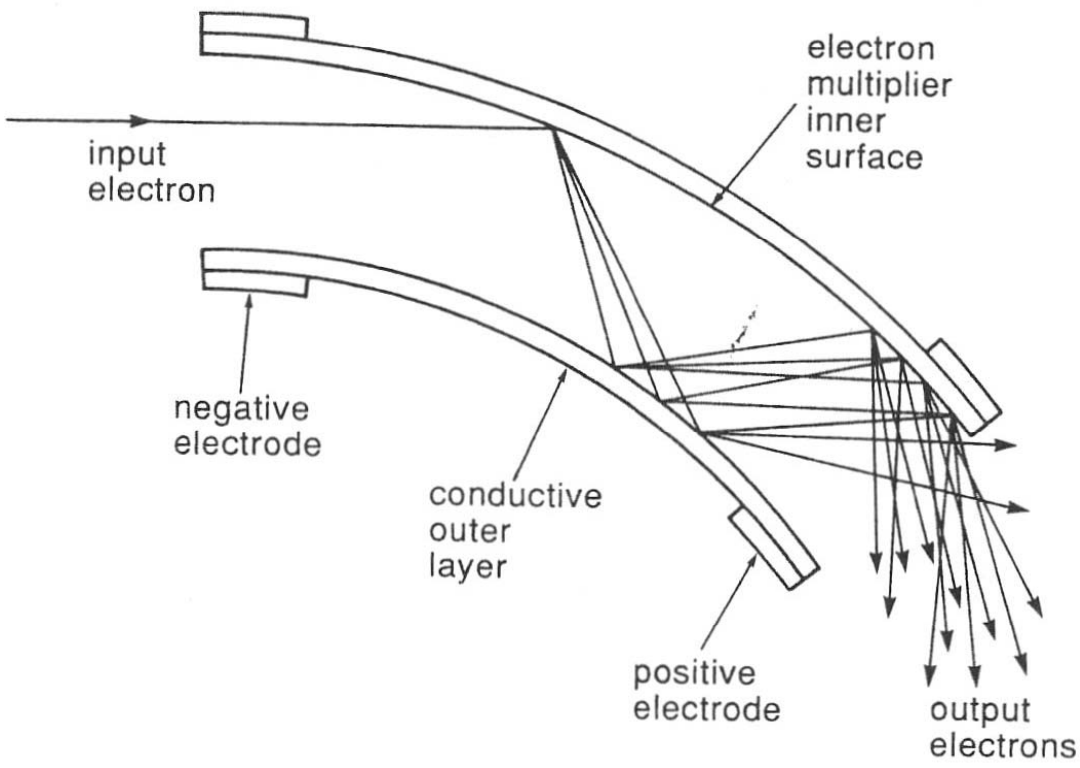

Figure 8.8. Operation of a single microchannel.

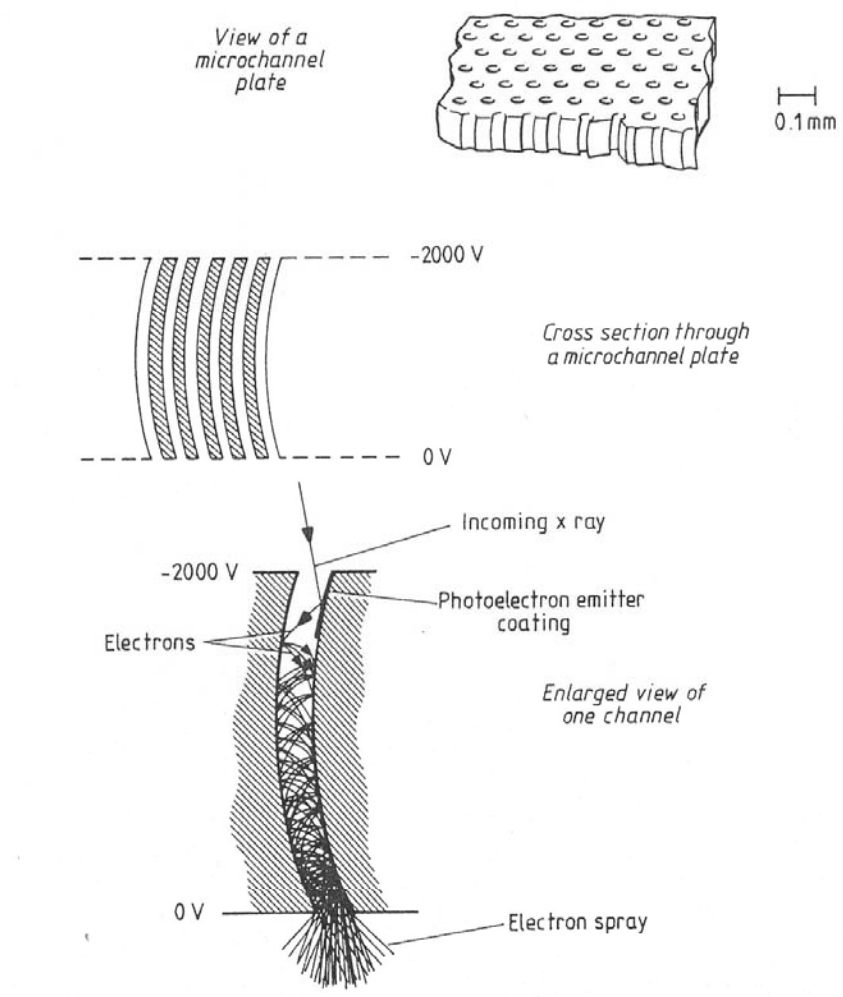

Figure 1.3.4 Schematic view of the operation of a microchannel plate.

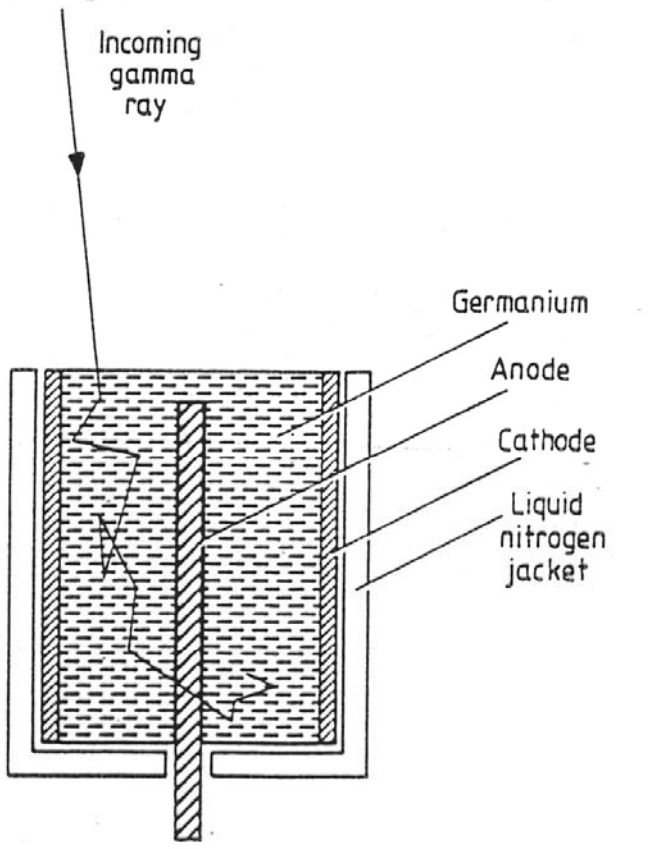

Figure 1.3.3 Germanium gamma-ray detector.

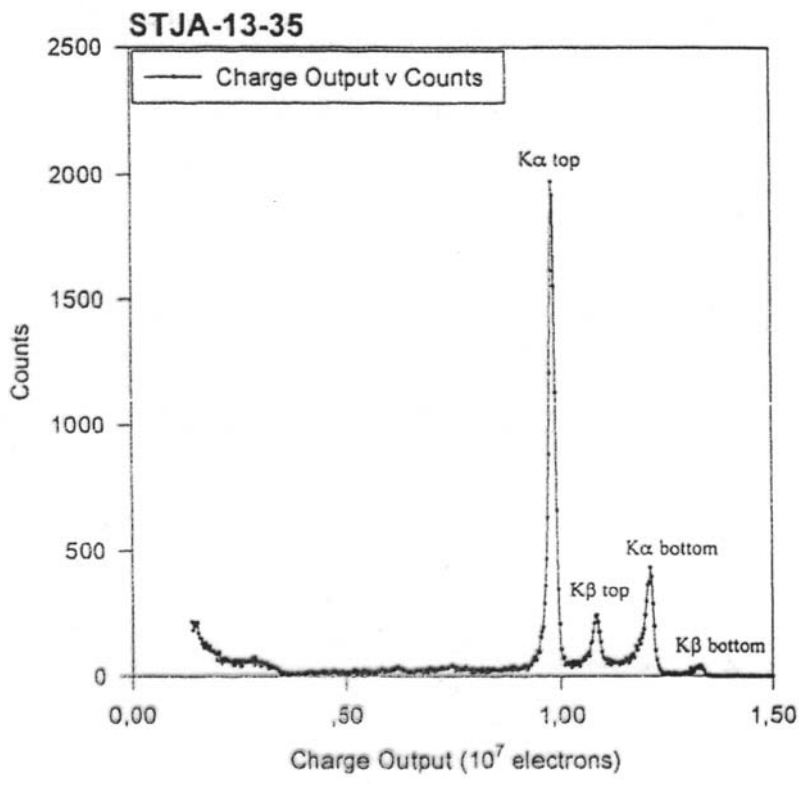

Chandra X-ray Observatory

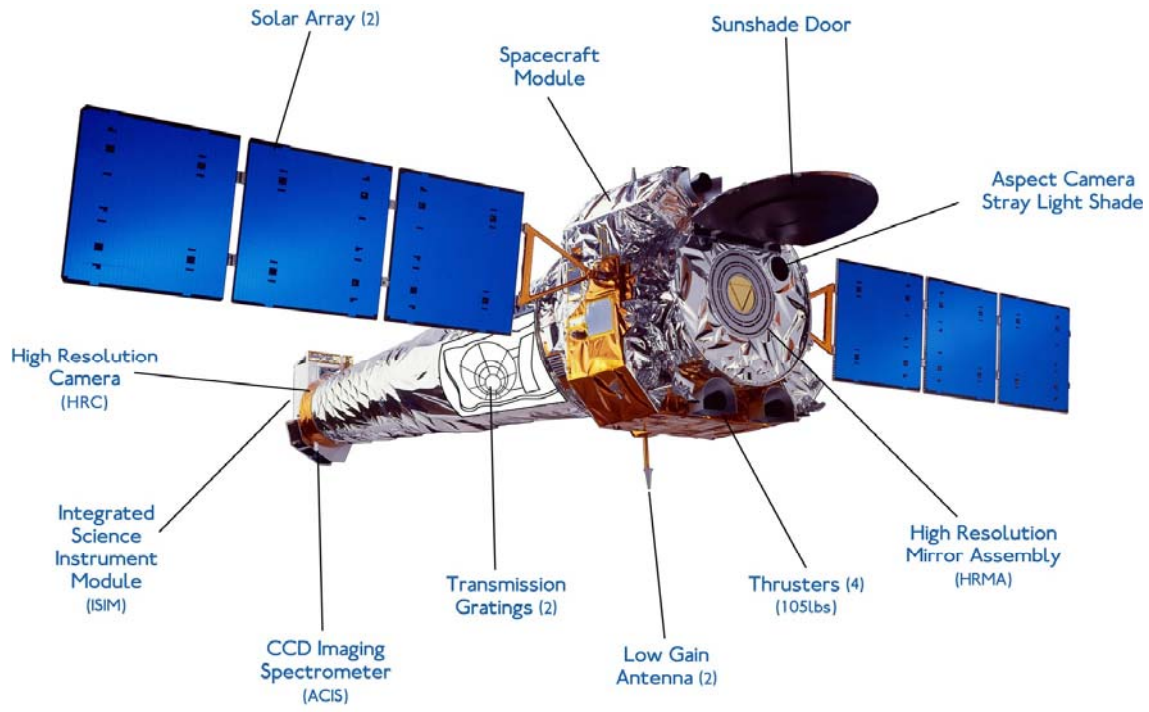

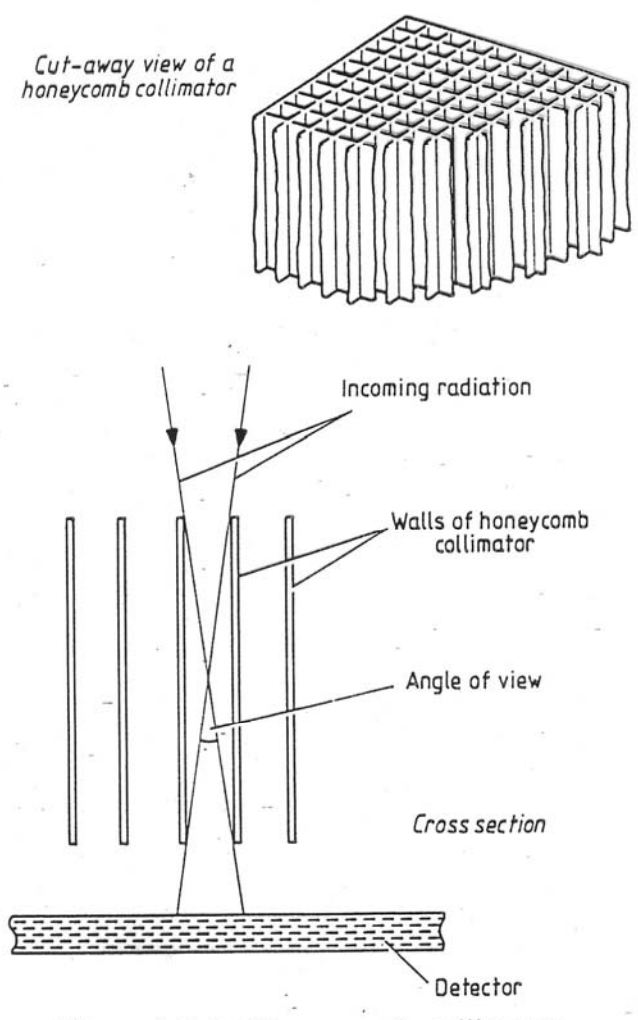

Figure 1.3.5 Honeycomb collimator.

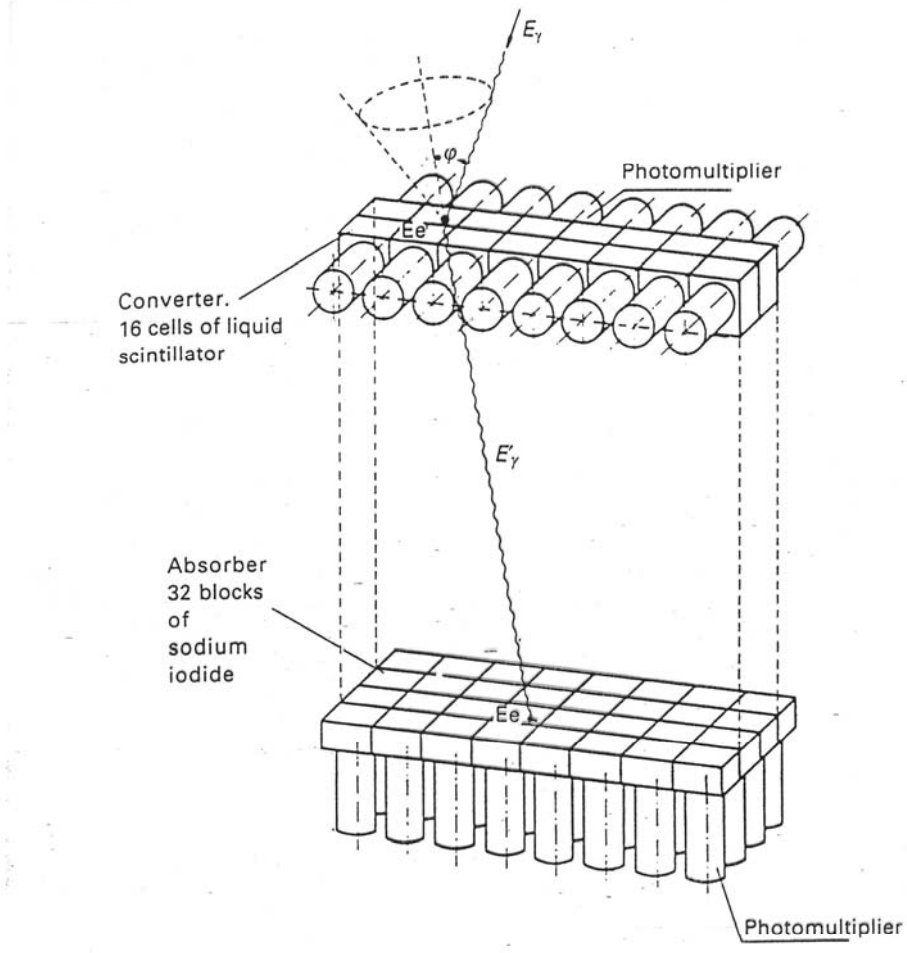

Figure 7.20. A schematic drawing of the MPIfEP Compton telescope for γ-rays, illustrating the principle of measuring the scattering angle ϕ. The distance between the converter and the absorber is 1.2 m. (From V. Schonfelder, F. Graml and F.-P. Penningsfeld (1980). *Astrophys. J.*, **240**, 350.)

Gas discharge tube

Geiger counter

Proportional counter

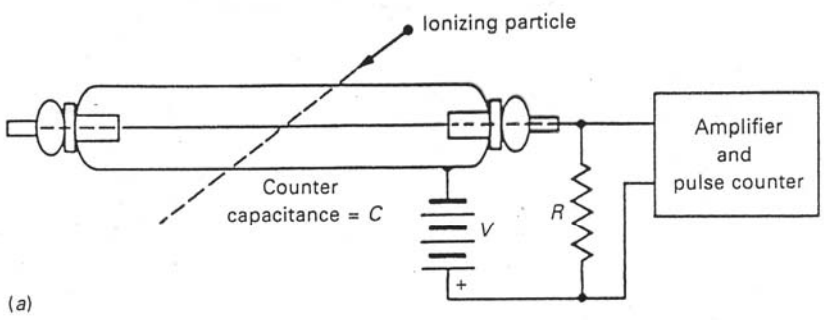

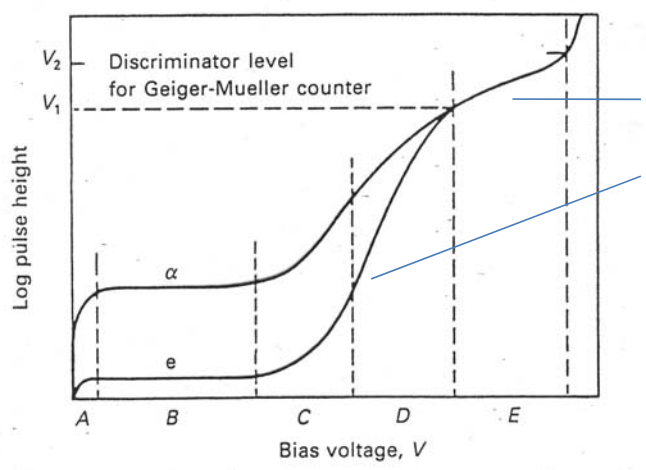

Geiger-Mueller: $G > 10^8$

Proportional: $G \sim 10^4 - 10^5$

For proportional counter: measure charge position along the central wire to get the charge position.

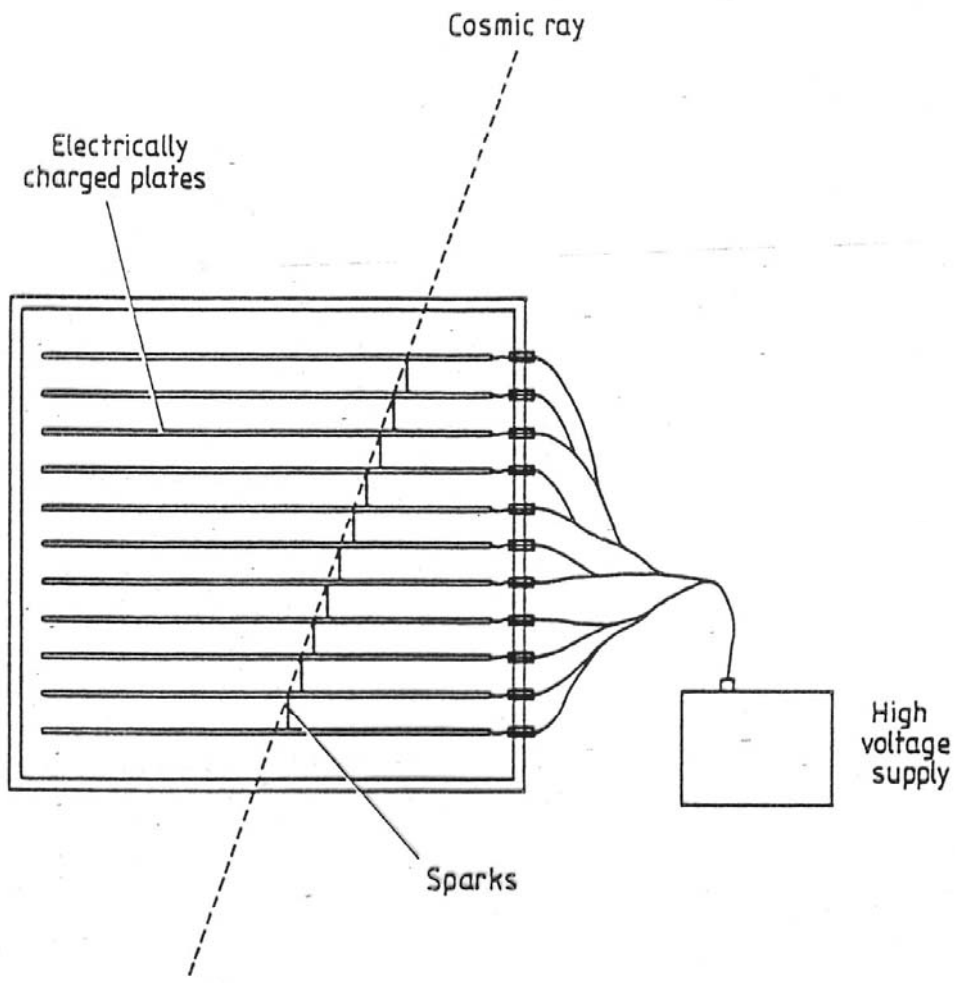

Figure 1.4.3 A spark chamber.

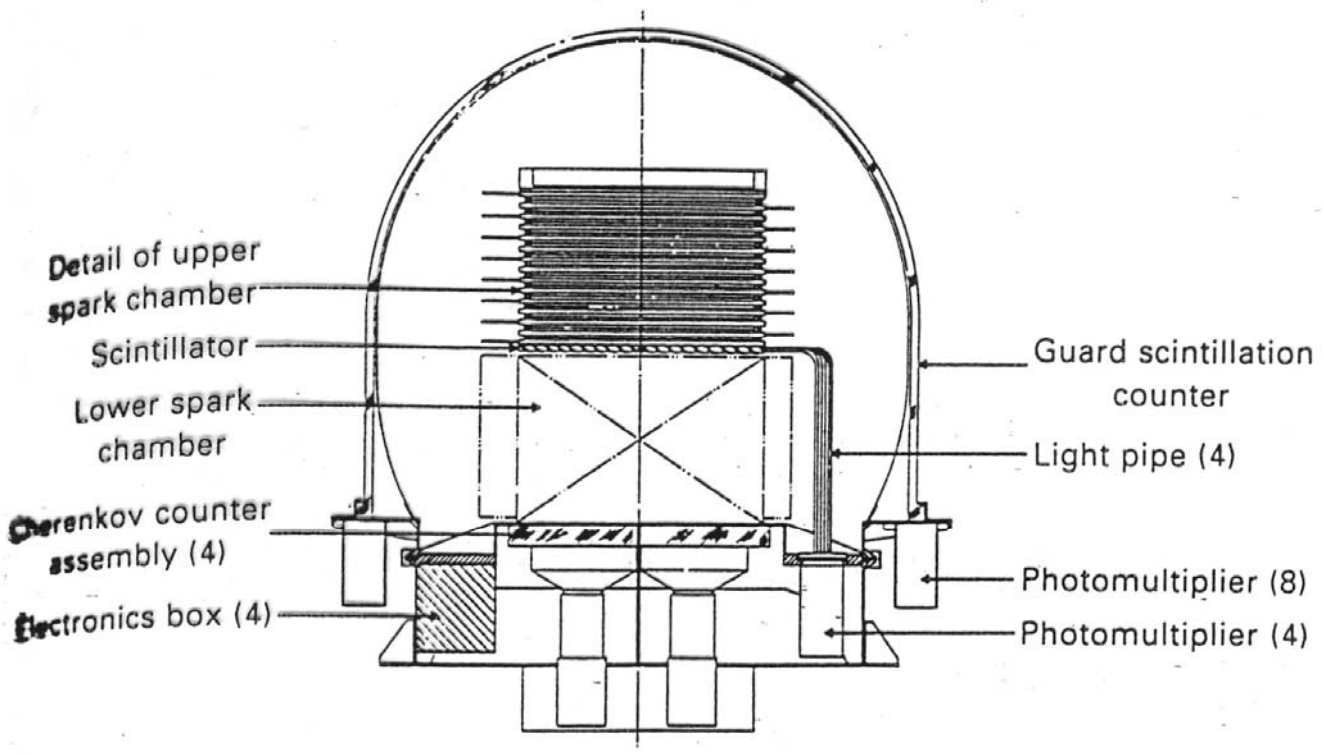

Figure 7.19. The SAS-II γ-ray telescope showing the arrays of spark chambers within the spherical anticoincidence shield. (From C. E. Fichtel (1974). *Phil. Trans. Roy. Soc. Lond.*, 277, 367.)

GLAST (Fermi) Detectors

Large Area Telescope
(20% sky coverage)

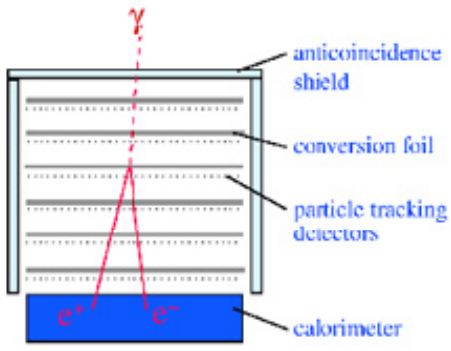

- Anticoincidence detector triggers on charged particles (so, not gamma-rays)
- W sheets convert gammas to e+/- pairs
- Silicon strip detectors track particles
- Calorimeter measures particle energies

GLAST Burst Monitor

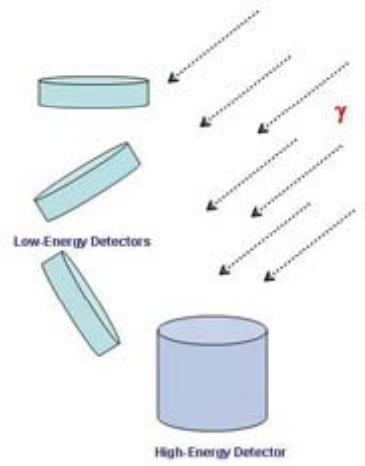

Twelve NaI low-energy (8 keV – 1 MeV) X-/gamma-ray detectors facing in different directions locate source within a few degrees. Two BiGeO calorimeters do much the same for high-energy (150 keV – 30 MeV) gamma rays.

First Fermi all-sky gamma ray map

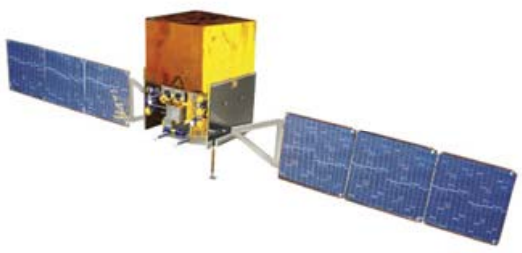

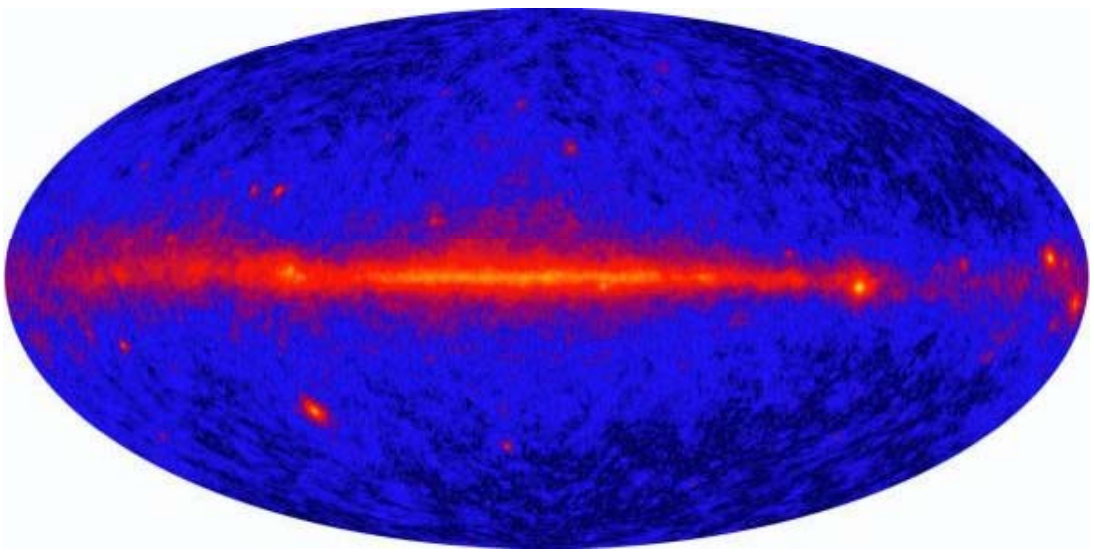

August 2008

Swift Satellite

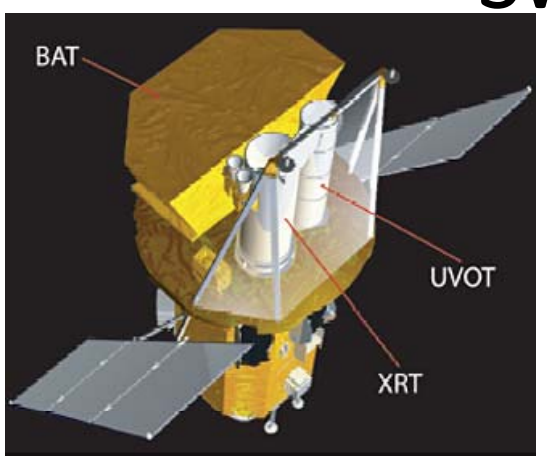

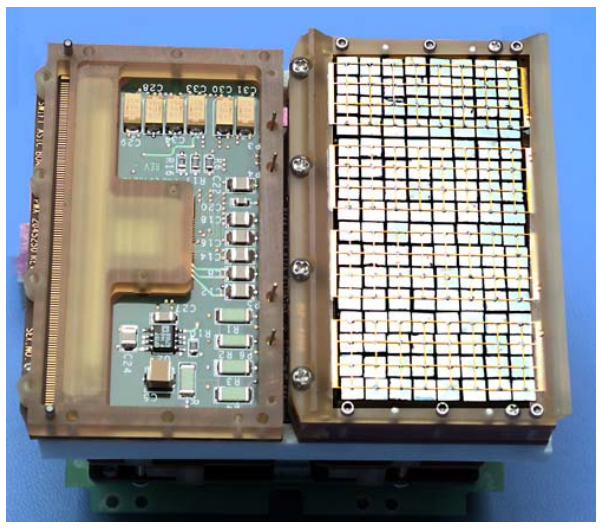

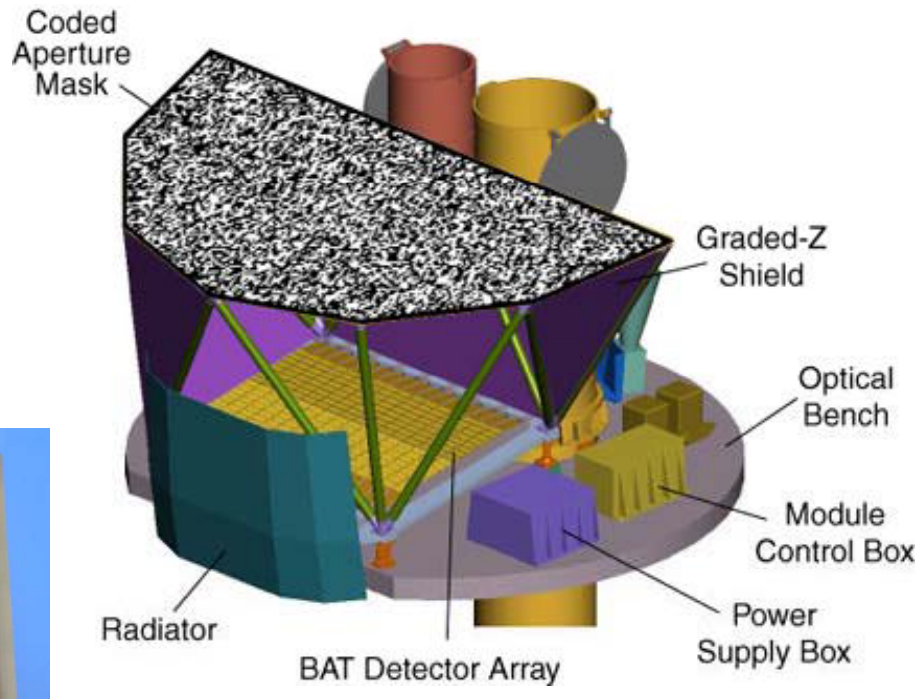

ZnCdTe calorimeter array (32,768 elements) and readout electronics

BAT coded-aperture mask

1.4 Sr field of view, 15-150 keV

Pierre Auger Observatory, Argentina

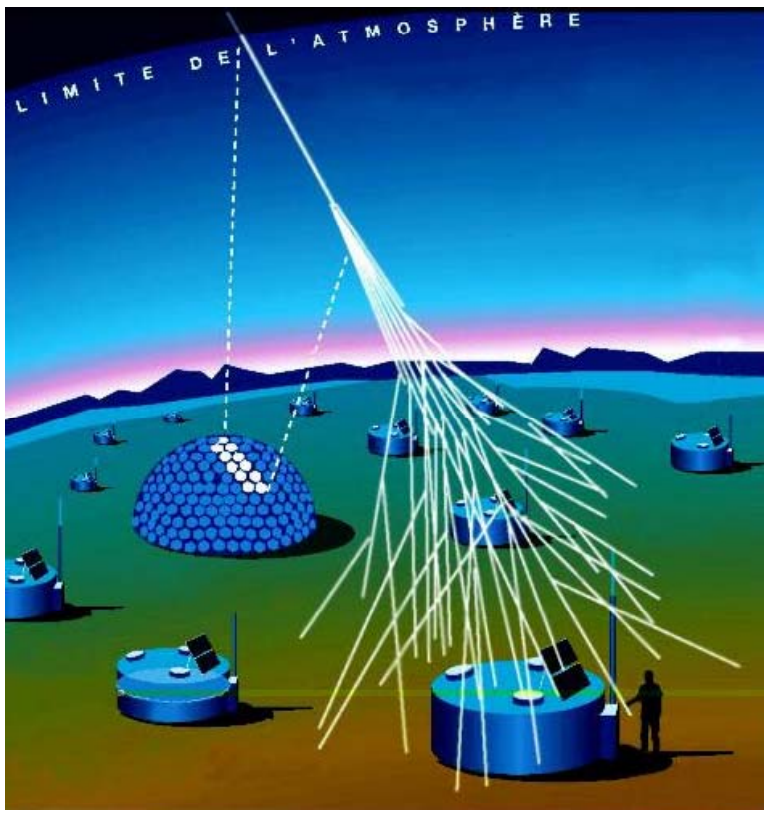

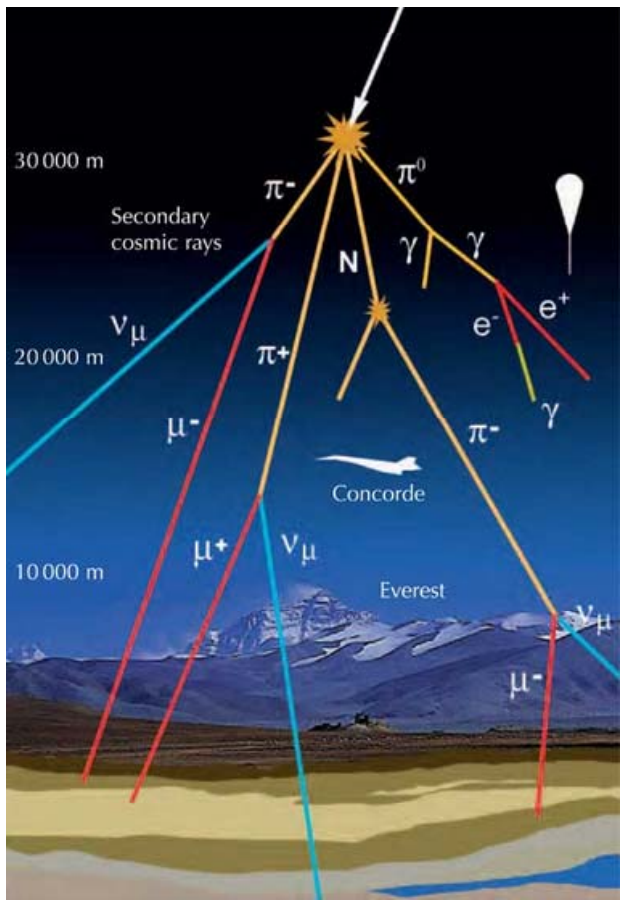

Air “fluorescence” (really luminescence or scintillation) and Cherenkov detectors for charged particles (cosmic rays)

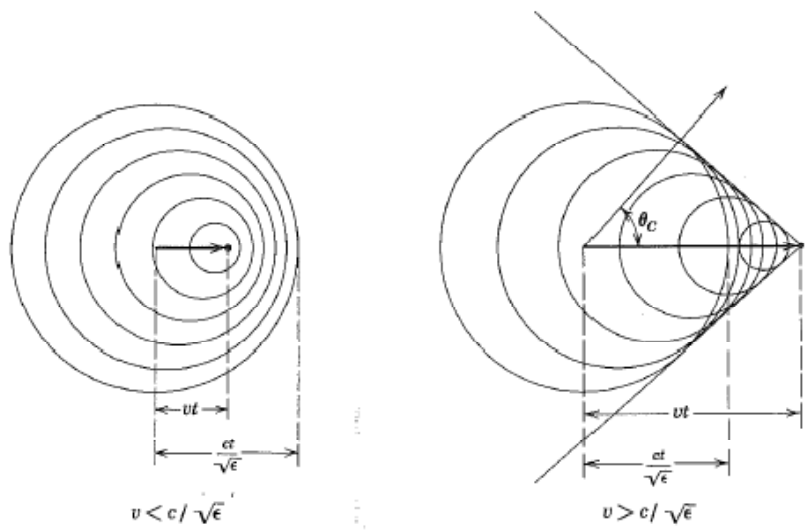

Fig. 13.8 Cherenkov radiation. Spherical wavelets of fields of a particle traveling less than and greater than, the velocity of light in the medium. For $v > c/\sqrt{\epsilon}$, an electromagnetic “shock” wave appears, moving in the direction given by the Cherenkov angle θ_C.

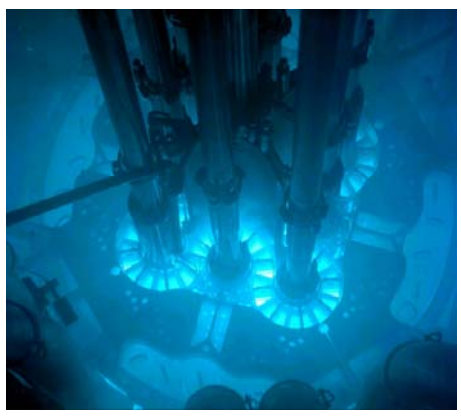

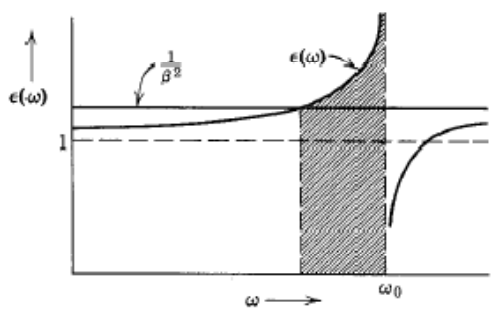

Fig. 13.6 Cherenkov band. Radiation is emitted only in shaded frequency range where $\epsilon(\omega) > \beta^{-2}$.

Jackson, “Classical Electrodynamics”

Cherenkov detectors

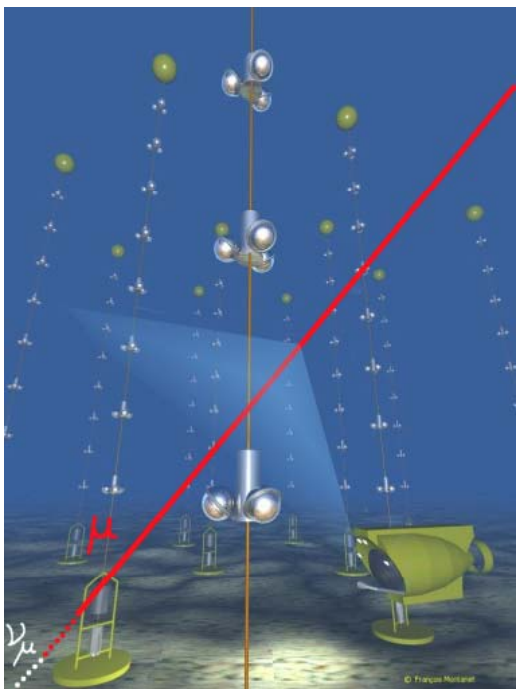

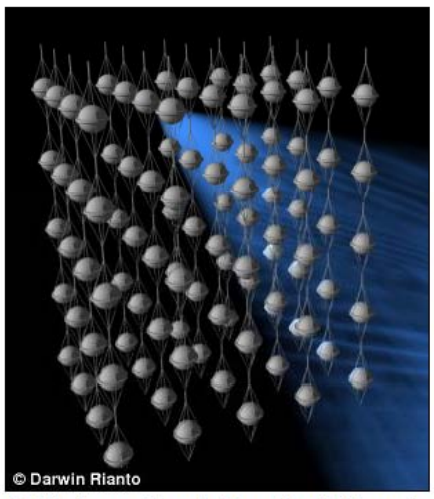

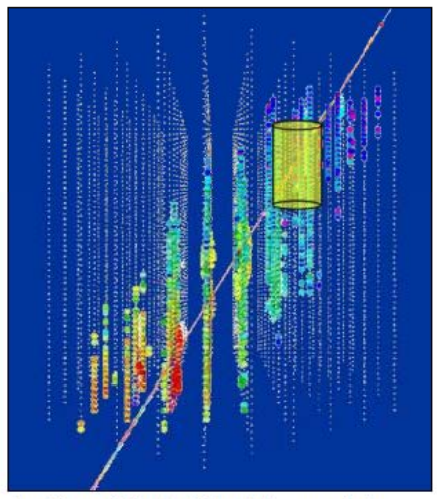

Artist's impression of a 'Cerenkov light cone' passing through the IceCube telescope, left. IceCube will encompass AMANDA (yellow cylinder), right, a smaller neutrino detector. The coloured dots show where the passage of a neutrino has been detected by the modules as it passes through the array

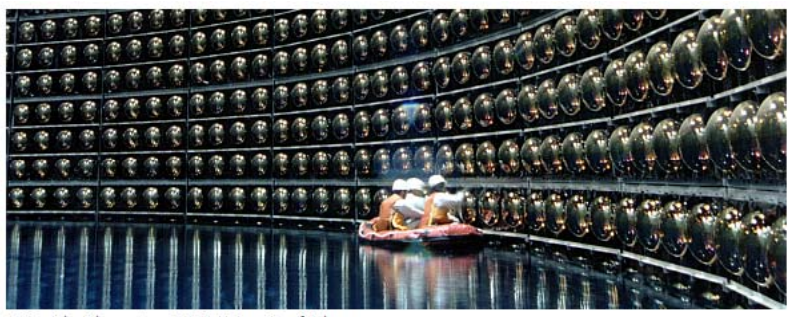

© Kamioka Observatory, ICRR, University of Tokyo
(Ausschnitt)

HAWC Observatory, Mexico
Ice Cube, South Pole

The HAWC Observatory (INAOE).

HAWC: cosmic ray detector

Ice Cube: neutrino detector